Melanopsin-driven increases in maintained activity enhance thalamic visual response reliability across a simulated dawn

Riccardo Storchi[a], Nina Milosavljevic[a], Cyril G. Eleftheriou[a], Franck P. Martial[a], Patrycja Orlowska-Feuer[b], Robert A. Bedford[a], Timothy M. Brown[a], Marcelo A. Montemurro[a], Rasmus S. Petersen[a], and Robert J. Lucas[a,1]

[a]Faculty of Life Sciences, University of Manchester, M13 9PT Manchester, United Kingdom; and [b]Department of Neurophysiology and Chronobiology, Institute of Zoology, Jagiellonian University, 30-387 Krakow, Poland

Edited by David M. Berson, Brown University, Providence, RI, and accepted by the Editorial Board August 27, 2015 (received for review March 16, 2015)

Twice a day, at dawn and dusk, we experience gradual but very high amplitude changes in background light intensity (irradiance). Although we perceive the associated change in environmental brightness, the representation of such very slow alterations in irradiance by the early visual system has been little studied. Here, we addressed this deficit by recording electrophysiological activity in the mouse dorsal lateral geniculate nucleus under exposure to a simulated dawn. As irradiance increased we found a widespread enhancement in baseline firing that extended to units with ON as well as OFF responses to fast luminance increments. This change in baseline firing was equally apparent when the slow irradiance ramp appeared alone or when a variety of higher-frequency artificial or natural visual stimuli were superimposed upon it. Using a combination of conventional knockout, chemogenetic, and receptor-silent substitution manipulations, we continued to show that, over higher irradiances, this increase in firing originates with inner-retinal melanopsin photoreception. At the single-unit level, irradiance-dependent increases in baseline firing were strongly correlated with improvements in the amplitude of responses to higher-frequency visual stimuli. This in turn results in an up to threefold increase in single-trial reliability of fast visual responses. In this way, our data indicate that melanopsin drives a generalized increase in dorsal lateral geniculate nucleus excitability as dawn progresses that both conveys information about changing background light intensity and increases the signal:noise for fast visual responses.

melanopsin | irradiance | neural coding | silent substitution | DREADD

The rotation of the earth imposes slow but very high amplitude changes in background light intensity (irradiance) across dawn and dusk. An array of light adaptation mechanisms acts to buffer the visual code against this substantial variation in its physical origins (1–8). Nonetheless, we certainly perceive the change in brightness of our environment, raising the question of how the visual system represents such gradual changes in irradiance.

The question of how the early visual system encodes background light levels has previously been addressed by extended exposure to spatially uniform stimuli. Under these conditions, many neurons in the retina and visual thalamus scale their maintained firing rate according to stimulus irradiance over many decades (9–14). This behavior, sometimes termed "luxotonic," implies that natural slow changes in irradiance would be represented by gradual modulations in firing rate across at least a fraction of the visual projection. However, we are unaware of a direct test of that prediction. Moreover, the extent to which luxotonic activity survives in the presence of higher-frequency visual stimuli (as would be the case in any natural scene) remains unknown. We start here by addressing these deficits and showing that naturalistic dawn transitions do indeed induce a diffuse increase in firing across the mouse dorsal lateral geniculate nucleus (dLGN).

Although the luxotonic capacity of the mammalian visual system has been appreciated for >50 y, both the retinal origins and functional significance of this mode of action remain controversial. An important question is how luxotonic changes in maintained firing impact the ability of neurons to encode other visual features. There is the obvious potential for increases in baseline firing to occlude other responses; it has also been suggested that luxotonic behavior could improve signal:noise for fast visual responses by regularizing firing patterns (9, 15; although see refs. 16 and 17). A second aim of this study was to resolve this controversy, by directly measuring responses to high-frequency visual stimuli across naturalistic ramps in irradiance.

Our final objective was to address the retinal circuitry responsible for luxotonic activity. Under mesopic and photopic conditions, cone photoreceptors track fast modulations in local luminance, with rapid alterations in membrane potential. However, they also can encode background light intensity with changes in steady-state voltage, and this signal can be propagated through the retinal circuitry to support luxotonic activity in ganglion cells and beyond (18–21). At brighter backgrounds, however, the photoreceptor steady state response approaches saturation (6, 22, 23). Under these conditions, further changes in maintained firing could be driven by intrinsically photosensitive retinal ganglion cells (ipRGCs), which can rely upon their intrinsic melanopsin-dependent light response to accurately encode higher irradiances (24). Here we used a combination of conventional knockout, receptor-silent substitution and chemogenetic manipulations to test the hypothesis that ipRGCs

Significance

Irradiance-dependent ("luxotonic") changes in baseline firing were first described in neurones of the early visual system decades ago. However, the origin and function (if any) of this visual response is still poorly understood. Here we address both questions by recording electrophysiological activity in mouse dorsal lateral geniculate nucleus over a simulated dawn. First, we show that in the photopic regime luxotonic activity becomes increasingly driven by inner-retinal melanopsin photoreceptors as irradiance increases. Then, that irradiance-dependent increases in activity apply not only to baseline firing but also to the amplitude of fast visual responses, producing increases in signal:noise across the simulated dawn, revealing a function for luxotonic activity and a new way in which inner retinal photoreceptors support conventional vision.

Author contributions: R.S., N.M., T.M.B., M.A.M., R.S.P., and R.J.L. designed research; R.S., N.M., C.G.E., F.P.M., P.O.-F., and R.A.B. performed research; R.S., N.M., M.A.M., and R.S.P. analyzed data; and R.S. and R.J.L. wrote the paper.

The authors declare no conflict of interest.

This article is a PNAS Direct Submission. D.M.B. is a guest editor invited by the Editorial Board.

Freely available online through the PNAS open access option.

[1]To whom correspondence should be addressed. Email: robert.lucas@manchester.ac.uk.

This article contains supporting information online at www.pnas.org/lookup/suppl/doi:10.1073/pnas.1505274112/-/DCSupplemental.

support responses to naturalistic changes in irradiance under these conditions.

Results

Luxotonic Activity in the Mouse dLGN. Previous work in a variety of species has used extended light steps to reveal luxotonic activity. In preliminary studies we found evidence that such stimuli induce irradiance-dependent increases in firing also in some neurons in the mouse dLGN (Fig. 1*A*). However, for this study we chose to use a simple ramp stimulus instead (Fig. 1*B*), because: (*i*) the absence of abrupt changes in irradiance should provide a more complete isolation of luxotonic firing from more transient visual responses (Fig. 1*C*), and (*ii*) it allows a closer approximation of a natural change in irradiance: the dawn transition. For the latter purpose we generated a light ramp, the spectral composition of which recreated the mouse's experience of natural light (*Methods*), and magnitude and rate of change captured elements of a dawn transition (Fig. 1*B*). When presented with this ramp, we found that many units in the contralateral dLGN showed a graded increase in firing (Fig. 1*C*). The monotonic relation between irradiance and the change in firing rate elicited by the ramp was quite different from the complex response to light steps (Fig. 1*A*), consistent with our prediction that this stimulus would more effectively reveal luxotonic activity.

At the single-unit level there was a very strong bias toward higher firing rates at the end of the ramp (Fig. 1*D* and *SI Appendix*, Fig. S1). There was no clear bimodality in this behavior, indicating a continuum of irradiance responsiveness (Fig. 1*D*). True irradiance coding requires a simple relationship between irradiance and firing rate across the ramp. To determine the extent to which this occurred, we computed the goodness-of-fit (R^2) of a the log:linear relation between firing rate and irradiance for all single units. The R^2 values would be high for units whose irradiance-related change in firing rate was large compared with any random variation, and low for units without a change in firing rate or with high variability. R^2 varied continuously across the population, again indicating that luxotonic activity was a general feature of the dLGN, apparent to at least some extent in many neurons, rather than segregated to a particular population (Fig. 1*E*). There was a positive correlation between R^2 and the increase in firing rate, revealing that by far the most prevalent irradiance responses were positive. This was also apparent in the normalized average firing rate of those units passing a reasonable criterion for classification as strongly luxotonic ($R^2 > 0.5$) (Fig. 1*F*). This population also showed good reproducibility in their response to multiple repeats of the ramp (Pearson's $\rho = 0.44 \pm 0.07$; $P = 1.5 \times 10^{-6}$, *t* test; $n = 27$). We found only two units (of 40) that had both a high R^2 and a reduction in firing rate across the ramp.

Therefore, 23% of dLGN units ($n = 40$ of 173 from six mice) were classified as having robust luxotonic activity ($R^2 > 0.5$) across the irradiance ramp. This likely is a conservative estimate, as it is based upon a single repeat of the stimulus, and the relatively long duration of the ramp allows ample opportunity for spontaneous fluctuations in activity (17, 25) to occlude the response. To assess the impact of the latter effect, we delivered a threefold faster version of the same ramp stimulus. Luxotonic activity was indeed more robust under these conditions, with 64% of units ($n = 178$ of 278 from five mice) having $R^2 > 0.5$ for the log:linear fit (Fig. 1 *G–I*).

These results suggest a widespread occurrence of luxotonic behavior across the dLGN. Histological reconstructions of recording sites showed that there was no clear spatial segregation of the irradiance response, with units with high R^2 values distributed widely across the dLGN (Fig. 1*J* and *SI Appendix*, Figs. S2 and S3). On occasion we also recorded units that were not light-responsive (in few cases within the dLGN, but mostly in more medial parts of the thalamus). These units were not included in the analyses reported throughout the paper. However, we used them to test the possibility that changes in firing rate observed in dLGN were not a product of some nonspecific changes in brain activity. Indeed we did not observe a net increase or decrease in time-averaged firing rate for these units (Fig. 1*K*).

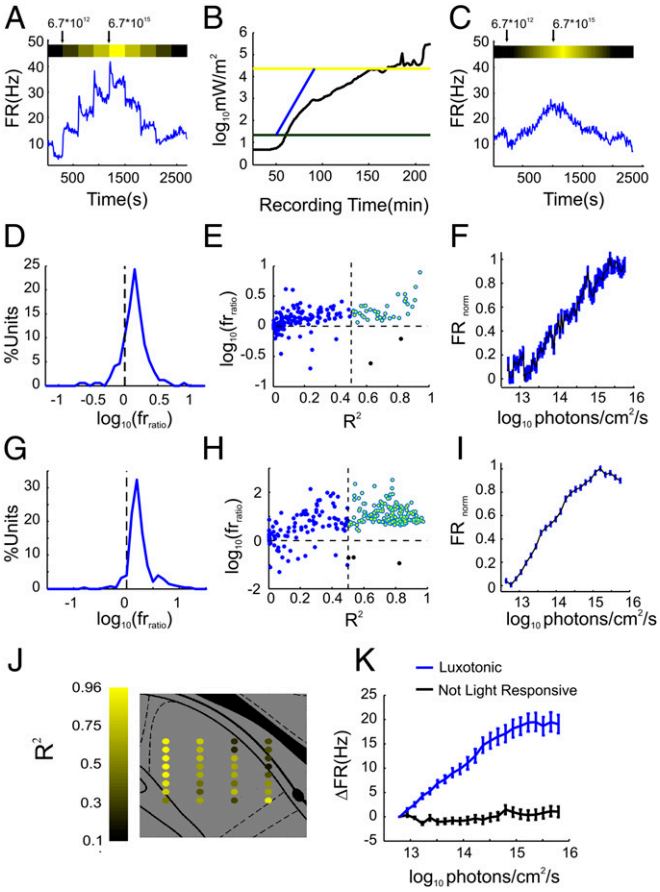

Fig. 1. dLGN responses to irradiance ramps. (*A*) Representative unit exhibiting changes in firing rate upon exposure to staircase changes in irradiance across three decades. Numbers above depict irradiance in photons per square centimeter per second. (*B*) Spectral power density across a dawn transition on a partially cloudy summer day. Irradiance reached the detection threshold of our meter around 5 mW/m^2 (12.71 $\log_{10}$ photons per square centimeter per second; −2.6° solar elevation, 44° solar azimuth) and increased by a further four decimal orders over the following 2 h. Across this time, rates of change varied from 0.1 to −0.1 $\log_{10}$ (mW·m^2·min). A simple irradiance ramp [log-linear increase in irradiance from 22.4–22,400 mW/m^2 or 0.6–3.6 $\log_{10}$ (melanopic lux) measured as in Lucas et al. (66) over 38 min, rate of increase = 0.08 $\log_{10}$ (mW/m^2)/min] was designed to recapitulate elements of a natural dawn transition (cyan line). (*C*) Representative unit exhibiting change in firing rate across a symmetrical increasing-decreasing ramp across three decades of irradiance (shown above in photons per square centimeter per second). (*D*) The largest fraction of units ($n = 141$ of 173) exhibits increase in firing rate between the lowest and highest irradiance levels (data are pooled at half-log unit steps in irradiance). The fr_{ratio} indicates the ratio between firing rate at lowest and highest irradiance (estimates performed on half-log unit intervals). (*E*) Strongly luxotonic units ($R^2 > 0.5$) show a positive relation with irradiance (yellow dots). (*F*) Normalized average response for the strongly luxotonic units (mean ± SEM normalized firing rate). (*G*) Same as in *D* for the fast-ramp stimulus ($n = 256$ of 276 show an increase in firing rate). (*H* and *I*) Same as in *E* and *F* for the fast-ramp stimulus. (*J*) Representative recording shows that luxotonic units could be found across large areas of the dLGN. The circles show reconstructed electrode locations against a coronal section of the mouse dLGN, the color code shows R^2 values at each site. (*K*) Units outside the LGN (mean ± SEM, $n = 36$) did not display a consistent change in firing across the fast ramp (black error bars). For comparison we reported the response of luxotonic units ($R^2 > 0.5$) from the same dataset (blue error bars).

The Role of Melanopsin and ipRGCs. We next turned our attention to the origin of the irradiance response, and in particular the contribution (if any) of melanopsin photoreception. For these studies we used the faster ramp, which revealed irradiance responses in more units. We first asked whether luxotonic activity is disrupted in mice lacking melanopsin (*Opn4*$^{-/-}$). When the ramp was applied to melanopsin knockout mice, we found that there was very little increase in dLGN firing rate across the irradiance ramp (Fig. 2 *A* and *B*; see *SI Appendix*, Fig. S4 for a distinction between ON and OFF responses in *Opn4*$^{-/-}$). We found that a few neurons ($n = 33$ of 252) met our criterion for classification as luxotonic ($R^2 > 0.5$) over a first presentation of the ramp (Fig. 2*C*), indicating retention of some luxotonic activity, although these showed poor reproducibility compared with intact animals (Pearson's $\rho = 0.25 \pm 0.1$ for *Opn4*$^{-/-}$ mice between first and second presentations, compared with 0.64 ± 0.03 for intact animals; $P = 1 \times 10^{-6}$, *t* test).

The *Opn4*$^{-/-}$ data are consistent with a melanopsin-contribution to luxotonic activity, but given the evidence of developmental abnormalities in this genotype (26–28), we wished to confirm this finding with other methods. We next assessed the impact of selective and acute inhibition of ipRGC activity using chemogenetics (29, 30) in visually intact mice. An AAV2 viral vector [AAV2-hSyn-DIO-hM4D(Gi)-mCherry] allowing cre-dependent expression of an inhibitory hM4D DREADD (designer receptors exclusively activated by designer drugs) receptor was introduced to the vitreal cavity of *Opn4*^{Cre}:Z/EGFP mice. After 6 wk, analysis of mCherry flourescence revealed that the transgene was expressed in a small number of cells in the inner nuclear and ganglion cell layers. Counterstaining for the GFP reporter expressed in ipRGCs revealed that about 30% of ipRGCs had been successfully transduced (Fig. 2*D*). mCherry-expressing cells had a variety of soma sizes and labeled dendrites stratified in both outer and inner sublamina of the inner plexiform layer, suggesting that multiple ipRGC subtypes had been targeted. To confirm that these Gi DREADD receptors were able to suppress ipRGC activity, we assessed the impact of its agonist (clozapine-*N*-oxide; CNO) on a known ipRGC output, the pupil light reflex. We found that systemic administration of CNO (10 mg/kg) inhibited the pupil light reflex of Gi DREADD-treated (Fig. 2 *E* and *F*) but not of control eyes not expressing the receptor (Fig. 2*F*). The effect was incomplete (consistent with the relatively small fraction of ipRGCs transduced) but persisted for tens of minutes, with substantial effects recorded at ∼30 min after injection (Fig. 2*F*) and partial recovery by 120 min (Fig. 2*E*).

We then compared dLGN responses to the fast ramp before and after CNO injection in both Gi DREADD-expressing and control conditions (10 mg/kg, i.p.). As might be predicted given the incomplete expression of Gi DREADDs in ipRGCs, we found that firing rates still increased across the dLGN following CNO injection (Fig. 2*G*) ($P = 7 \times 10^{-21}$ and 2×10^{-5} *t* test, respectively, before and after CNO). However, Gi DREADD-activation did disrupt luxotonic behavior. There was a statistically significant reduction in the increase in firing across the ramp following CNO injection in Gi DREADD-expressing (Fig. 2*G*) ($P = 5 \times 10^{-4}$ paired *t* test) but not in control mice ($P = 0.67$ paired *t* test) (*SI Appendix*, Fig. S5*B*) and examination of single-unit responses indicated that the more dramatic effect was that the increase in firing across the ramp became less ordered. This result can be observed both in a representative example in Fig. 2*H* and at the population level, where R^2 for the log:linear fit was significantly reduced 30 min after CNO administration in Gi DREADD-expressing animals (Fig. 2*I*) ($P = 4 \times 10^{-8}$ sign-test) but not in controls (Fig. 2*J*) ($P = 0.18$ sign-test). Similarly, the reproducibility of ramp responses after CNO injection in those units with the strongest luxotonic behavior ($R^2 > 0.5$) was also substantially reduced by CNO in DREADD mice in comparison with control mice (Fig. 2*K*) ($P = 2 \times 10^{-11}$). The effects of CNO were partially reversible, with some recovery in ramp response after 120 min ($P = 1 \times 10^{-7}$ sign-test) (*SI Appendix*, Fig. S5*D*).

As a final test of melanopsin's contribution to luxotonic activity, we explored the spectral sensitivity of this response. For this test, we took advantage of a recently published method using changes in spectral composition to selectively modulate effective irradiance for cones vs. melanopsin (31, 32). We thus adjusted the spectral power distribution of our original fast ramp stimulus (termed "Daylight" here because it recreated the mouse's experience of natural conditions) in such a way as to make it appear ∼10× dimmer for melanopsin across the whole ramp ("MelLow" ramp), without altering its appearance for cones (Fig. 2*L*; see *Methods* for details and ref. 32 for detailed validation of this approach). If melanopsin contributed to the irradiance sensitivity of the dLGN, we would therefore expect the change in firing rate to be temporally delayed for this new MelLow ramp. This was indeed what we observed. We used a protocol in which a MelLow ramp was presented in between two Daylight ramps. Firing rates increased across both types of ramp (Fig. 2*M*) ($P = 7 \times 10^{-47}$ and $P = 4 \times 10^{-33}$, respectively, for Daylight and MelLow). Units with strong luxotonic activity ($R^2 > 0.5$) were identified on the basis of their response to a first Daylight ramp. Across this group we were then able to compare the profile of the increase in firing to this first presentation of the ramp with subsequent presentation of MelLow and Daylight ramps. Responses to the two Daylight ramps were comparable (Fig. 2*N*). In contrast, there was a substantial discontinuity in the response to the intervening MelLow ramp, with the steepest component of the irradiance response shifted to later times (Fig. 2*N*), as expected if melanopsin were a significant determinant of luxotonic behavior. Whereas the MelLow spectrum was also ∼5× dimmer for rods, as their maintained membrane potential should be close to saturation across all of the light levels used here (33), it is most unlikely that they could contribute to encoding the slow change in irradiance. This assumption is consistent with the lack of luxotonic responses under these conditions in *Opn4*$^{-/-}$ mice.

The Impact of Spatiotemporal Contrast on Luxotonic Responses. The widespread appearance of luxotonic responses in the dLGN implies that the neurons exhibiting such behavior should also encode other visual features. This in turn raises the question of how dLGN units deal with slow changes in irradiance when they co-occur with other visual patterns. We first asked whether luxotonic changes in maintained firing are even apparent in the presence of other visual patterns by superimposing either a full-field white noise (ffWN), a naturalistic movie (NM), or a spatiotemporal white noise (stWN) to the slow ramp.

Consistent with the different statistics of these stimuli (see text in *SI Appendix* and *SI Appendix*, Fig. S13), an assessment of individual spike trains indicated that ffWN and stWN elicited numerous sharp changes in spiking activity (Fig. 3 *A* and *G* and *SI Appendix*, Fig. S6), but smoother changes were observed with the movie (Fig. 3*D*). Nevertheless, gradual increases in firing associated with ramp progression were retained in all conditions (Fig. 3 *B*, *E*, and *H*). Indeed, the incidence and magnitude of such responses to the ramp was at least as great as that observed with the slow ramp alone. Thus, in each case, at least 30% of units (32% for ffWN, $n = 70$ of 219; 30% for NM, $n = 34$ of 112; 52% for stWN, $n = 24$ of 46) met our criterion for classification as strongly luxotonic ($R^2 > 0.5$ for the log-linear fit) (Fig. 3 *C*, *F*, and *I*). Moreover, the proportional increase in firing among these units was similar to that observed for the simple slow ramp under all conditions (ffWN: $67.52 \pm 5.87\%$, $P = 0.15$, *t* test; NM: $98.63 \pm 10.19\%$, $P = 0.63$, *t* test; stWN: $116.85 \pm 13.63\%$ $P = 0.24$, *t* test). This finding indicates that, even in the presence of other visual stimuli, the irradiance ramp is an important determinant of time-averaged firing.

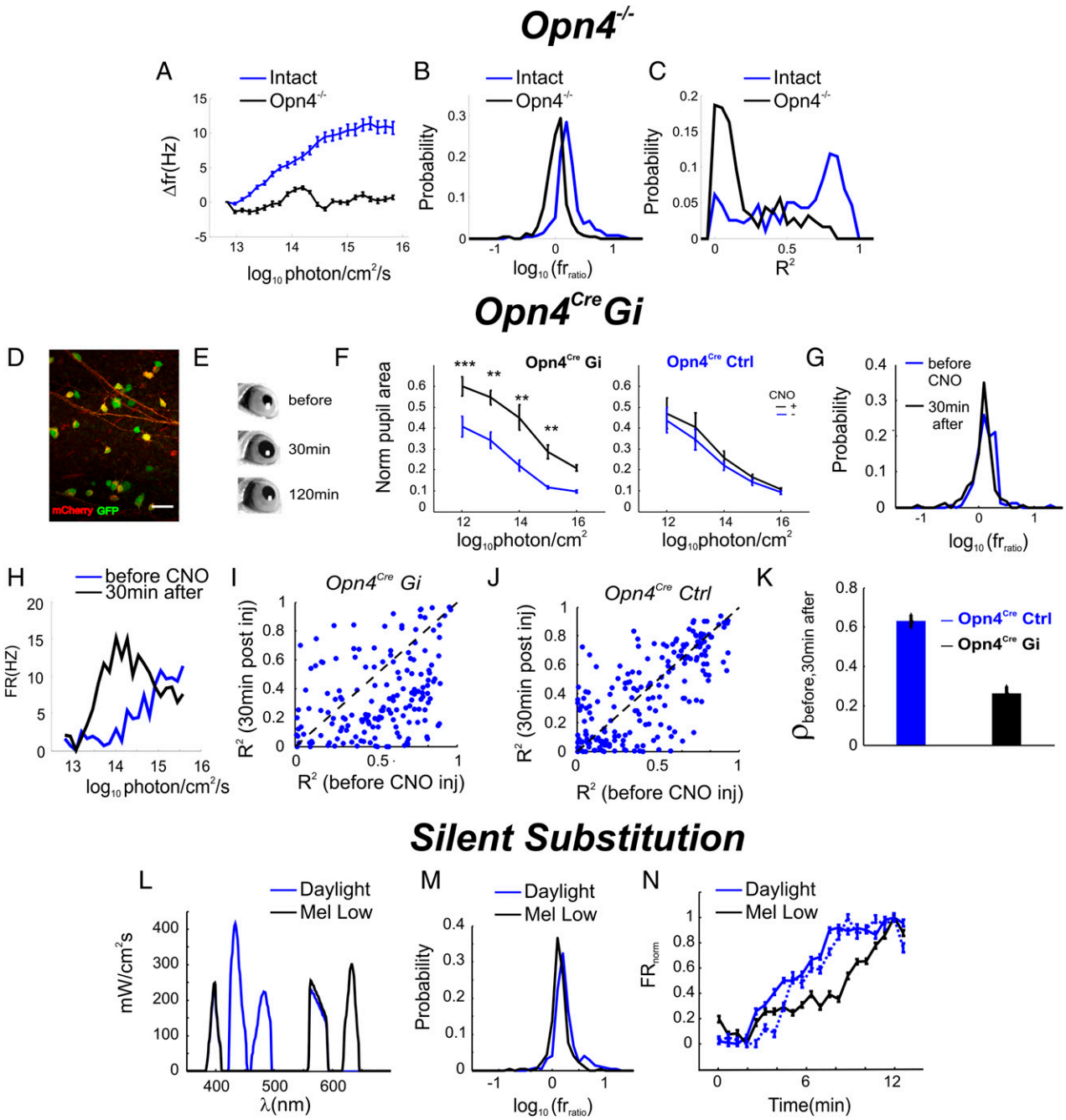

Fig. 2. Irradiance responses are defined by ipRGC and melanopsin. *Opn4*$^{-/-}$ mice lacked consistent luxotonic responses. (*A*) Normalized average response (mean ± SEM, $n = 252$) for dLGN units in *Opn4*$^{-/-}$ mice. (*B*) The increase in firing rate between the lowest and brightest ramp condition (data are pooled at half-log unit intervals in irradiance) was strongly reduced in *Opn4*$^{-/-}$ mice. (*C*) R^2 distribution in intact (blue) and *Opn4*$^{-/-}$ mice (black). The log-linear relation between irradiance and firing rate was substantially disrupted in *Opn4*$^{-/-}$ mice. (*D*) Following intravitreal injection of AAV2-hSyn-DIO-hM4D(Gi)-mCherry to *Opn4*^{Cre}:Z/EGFP mice, immunohistochemical staining revealed mCherry (red) expression in GFP^{+} neurons (green) in the ganglion and inner nuclear layers in retinal flatmounts. (Scale bar, 20 μm.) (*E*) Representative frozen video images of the mouse eye under high irradiance (10^{14} photons per square centimeter per second) shows substantial pupil dilation 30 min after CNO injection and partial recovery after 120 min. (*F*) CNO application (10 mg/kg, i.p.) inhibited pupil constriction (pupil area normalized to prepulse size; $n = 8$ mice) across a range of irradiances in *Opn4*^{cre} mice expressing Gi DREADD (*Left*) but not control (*Right*) animals not expressing DREADD (mean ± SEM). (*G*) Firing rate response is only partially inhibited by CNO application ($P = 7 \times 10^{-21}$ and 2×10^{-5} *t* test, respectively, before and after CNO). (*H*) Representative unit from the dLGN of *Opn4*$^{Cre/+}$ hM4D(Gi) expressing mice exposed to a fast irradiance ramp reveal that the firing rate response before CNO administration (cyan line) was substantially disrupted 30 min after injection (black line). (*I*) At the population level this is reflected in a reduction in R^2 for the log-linear fit of irradiance vs. firing rate 30 min after CNO injection ($R^2 = 0.52 \pm 0.02$ and 0.35 ± 0.02 mean ± SEM before and 30 min after CNO injection; $P = 2 \times 10^{-11}$, paired *t* test; $n = 166$). (*J*) These effects of CNO were absent in control mice not treated with the virus. (*K*) The impact of hM4D(Gi) activity is also apparent as a reduction in reproducibility of firing rate response of luxotonic units ($R^2 > 0.5$) after CNO injection in virus-treated vs. control mice (Pearson's $\rho = 0.26 \pm 0.04$ and 0.63 ± 0.03 respectively from $n = 91$ units in five virus-treated mice and from $n = 86$ in six control mice; $P = 2 \times 10^{-11}$, *t* test). (*L*) Irradiance spectrum of Daylight and MelLow stimuli. (*M*) MelLow ramp resulted in a slightly reduced increase in firing rate ($P = 3 \times 10^{-17}$ *t* test). (*N*) Activity of strongly luxotonic units (mean ± SEM; $n = 89$ from 4 mice) reveals that, although firing rate responses to multiple presentations of the original ramp recapitulating natural conditions were consistent (Daylight, solid and dashed lines represent, respectively, first and second presentation of the Daylight ramp; the second presentation occurred after the MelLow ramp), increases in firing were delayed when the spectral composition of the stimulus was changed to reduce the effective irradiance for melanopsin.

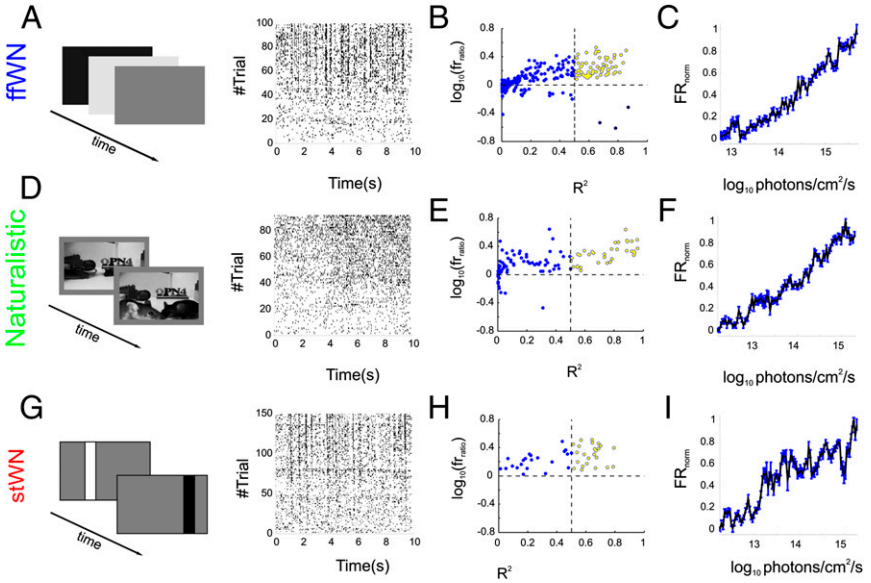

Fig. 3. Irradiance response is retained in the presence of other visual stimuli. (*A*, *D*, and *G*) Binarized trial bin counts for representative luxotonic units in response to repeated presentations of the ffWN (*A*), NM (*D*), and stWN (*G*) across the slow irradiance ramp. Example frames for ffWN, NM, and stWN are reported (*Left*). (*B*, *E*, and *H*) Relative increments in firing rate between lowest and highest irradiance across the ramp (respectively ffWN, NM, and stWN). (*C*, *F*, and *I*) Associated normalized firing rate profiles (mean ± SEM) for all strongly luxotonic units.

Inclusion of the ffWN stimulus also allowed us to classify the dLGN neurons as ON or OFF types based upon their temporal receptive field. As recently shown, this method of classification has the important advantage of returning consistent results across irradiance levels, whereas the ON-OFF profile of responses to simple steps is labile (34). Accordingly, units segregated into consistent ON or OFF types across irradiance levels. Objective analysis of temporal receptive fields (see *STA Clustering* in *Methods*) returned three types; two classes of ON-type receptive fields (one whose amplitude was strongly dependent upon irradiance), and a single OFF-type (Fig. 4*A*). As previously reported (35), the ON types were more numerous ($n = 70$ of 85). The average response to the ramp in all three categories was an increase in firing (Fig. 4 *B*–*D*). In addition, units with robust luxotonic activity were found in each group and in all cases had a positive relationship between time-averaged firing and irradiance (Fig. 4 *E*–*J*).

Impact of Luxotonic Responses on Fast-Evoked Responses. We finally turned our attention to how luxotonic increases in baseline firing rate impact fast-evoked visual responses. There are many reasons to expect that responses to superimposed visual stimuli might become more apparent across the ramp, not least because the absolute magnitude of luminance modulations must increase to keep relative amplitude (contrast) constant. However, irradiance-dependent increases in baseline firing might be expected to have the opposite effect by partially occluding fast responses. We therefore explored the relation between luxotonic increases in time-averaged firing and the reproducibility of firing patterns to single presentations of our high-frequency visual stimuli.

To this end, we computed the Pearson's correlation index (ρ) for repeated presentations of the fast stimuli across the ramp. Concentrating first on those units with the strongest luxotonic activity ($R^2 > 0.5$), we found that ρ increased as a function of irradiance for all of our high-frequency visual stimuli (ffWN, NM, and stWN) (Fig. 5*A*). The same was true if we used a looser definition of luxotonic activity and simply included all units with an increase in firing across the ramp (*SI Appendix*, Fig. S7). To determine the extent to which this effect was related to their luxotonic behavior, we asked whether it also occurred in units that showed no increase in firing rate across the ramp. For this analysis, we used the ffWN dataset as we found only few units whose firing rate did not increase across the ramp for the other stimuli (NM and stWN) (Fig. 3 *E* and *H*). Under ffWN, we found a small number of units with a log:linear reduction in firing rate ("negative luxotonic," $n = 3$; $R^2 > 0.5$) and a larger population whose firing rate was lower at the end of the ramp than the beginning ($fr_{\text{ratio}} < 1$) (Fig. 5*B*). In both groups, ρ was on average greater than in the luxotonic population at low irradiance, confirming that they responded well to high-frequency stimuli. Importantly, however, these units did not show an increase in ρ across the ramp (Fig. 5*B*) ($P = 0.31$ one-way ANOVA). Indeed, ρ decreased across the ramp in units with negative luxotonic behavior (Fig. 5*B*, dotted line). Overall, these results suggest that luxotonic increases in firing are required for irradiance-dependent improvements in the reproducibility of firing patterns under repeated presentations of the fast visual stimuli.

Next we asked which aspect of fast visual responses was responsible for the increase in single-trial reproducibility. Improvements in ρ could arise either from reductions in the variance of firing patterns or increases in the amplitude of fast responses. It has previously been proposed that luxotonic behavior regularizes patterns of baseline firing (9, 10, 15). We explored this possibility for our data by computing the Fano factor (variance/mean firing rate) across our simple slow-ramp stimulus. Fano factor was lower in units with strongest luxotonic behavior (Fig. 5*C*; see also *SI Appendix*, Fig. S8), but was invariant across the ramp (Fig. 5*C*) ($P = 0.98$ and 0.92 one-way ANOVA respectively for luxotonic and all units). In contrast, when ramps included high-frequency stimuli, there was a small reduction in Fano factor as the ramp progressed (Fig. 5*D*) (for all units: 2%, 4%, and 10%, $P = 0.06$, 0.16, 3×10^{-6}, one-way ANOVA; for luxotonic units: 8%, 8%, and 5%, $P = 0.003$, 0.07, 0.02, one-way ANOVA; ffWN, NM, and stWN stimuli, respectively).

We next turned our attention to the other potential origin for improvements in ρ: increases in the amplitude of responses to the fast visual stimuli. Across the ffWN ramp, we found a strong positive correlation between baseline firing rate and response amplitude across each repeat of the ffWN stimulus (shown for a representative luxotonic unit in Fig. 5*E* and across the population of dLGN units in

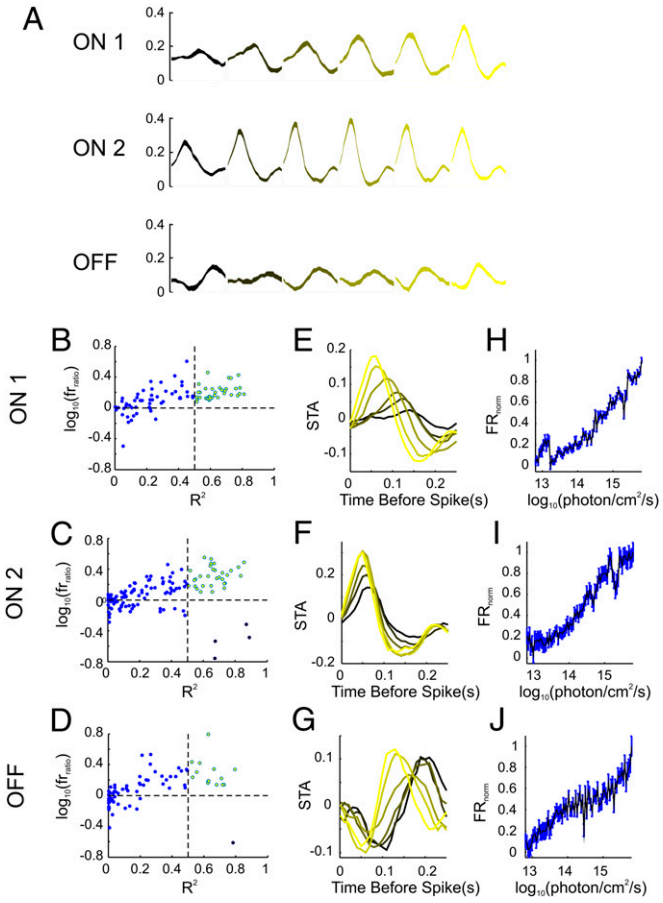

Fig. 4. Excitatory responses to ramp progression in both ON and OFF units. (*A*) Mean ± SEM of STAs from the three identified classes of dLGN units. Black-to-yellow color code indicates the transition from lowest to highest irradiance across the ramp. (*B–D*) Firing rate increased across the ramp for all unit types. (*E–J*) Average STAs (*E–G*) and normalized average responses (*H–J*) for the strongly luxotonic units ($R^2 > 0.5$).

Fig. 5*F*, *Left*). This was present in the most luxotonic units and also in those whose baseline firing rate did not change across the ramp (Fig. 5*F*, *Center* and *Right*), indicating that it was a general feature of dLGN physiology. Similar results were obtained for our other visual stimuli (*SI Appendix*, Fig. S10). These effects did not reflect slow adaptation to appearance of the stimulus but were a genuine response to the ramp because they were retained when the ramp stimulus was preceded by 20-min exposure to ffWN at the lowest irradiance (*SI Appendix*, Fig. S9).

The strong relation between baseline firing rate and fast-response amplitude provides a simple origin for the improvement in single-trial reproducibility across the ramp, suggesting that additional spikes are used to encode high-frequency stimuli when present. The magnitude of this effect can be large as ρ decreases linearly with baseline firing but increases quadratically with response amplitude (*SI Appendix*). Therefore, ρ would increase as long as the relative increase in response amplitude is larger than the square root of the relative increase in baseline firing rate. Indeed, this was the case for all our stimuli as the relation between response amplitude and baseline firing followed a power law whose exponent was >0.5 in all conditions (ffWN: exponent was 0.75, 0.74, 0.72 for *Left*, *Center*, and *Right* panels of Fig. 5*F*, respectively; for all dLGN units recorded during NM and stWN, the exponent was, respectively, 0.76 and 0.71). These results suggest that enhancements in response amplitude are a much bigger contributor to the luxotonic improvement in ρ than the regularization in firing pattern revealed in the Fano factor analysis. To determine whether this was the case, we estimated how ρ would change across the ramps if Fano factor values were held constant at the levels observed for the lowest irradiance (*SI Appendix*). As expected, the great majority of the increase in ρ was retained for all our stimuli, indicating that under all conditions the increase in response amplitude is the major origin of irradiance-dependent increases in ρ (Fig. 5*G*).

It seems then that increase in reproducibility for fast visual responses, mainly because of improvements in response amplitude, is inextricably tied to increases in baseline firing rate. This effect is consistent with the view that luxotonic activity reflects an irradiance dependent increase in excitability that impacts both baseline firing and fast-evoked responses and, as a result, increases response reproducibility.

Discussion

Luxotonic Activity in the Mouse dLGN. Here we have shown that an irradiance ramp that simulates a dawn transition induces a generalized and reproducible increase in firing across the mouse dLGN. This occurs in the artificial situation in which the ramp is the only visual feature presented and also when a variety of higher-frequency visual stimuli are superimposed upon it. The effect we see is analogous to the reported changes in maintained firing under extended exposure to spatially uniform stimuli often termed luxotonic. The ramp we use has several advantages for revealing such behavior. First, it has a straightforward relationship with a commonly experienced event: the dawn transition. Second, it allows isolation of responses to the very slowest changes in irradiance. Under natural viewing, the amount of light falling on the retina changes over many timeframes and, as the retina contains circuit elements with different temporal frequency tuning, there is likely a continuum between phasic and tonic modes of activity. Indeed, the representative unit in Fig. 1*A* takes several minutes to reach a stable firing rate after each step in irradiance. The ramp avoids this potential confusion by excluding abrupt changes in irradiance and providing a rate of change well outside that in which information about spatial patterns is conveyed.

A final advantage of the ramp protocol is that it allows the irradiance tracking behavior of single units to be quantified in a single metric: R^2 for a log-linear relationship between irradiance and firing rate. Others have reported that luxotonic activity occurs in large fractions of dLGN units (36). Our data are broadly consistent with this, because up to ∼60% of dLGN units meet a conservative criterion for having a luxotonic response ($R^2 > 0.5$ for log-linear fit). However, using the ramp protocol we see no evidence of a clear distinction between luxotonic and non-luxotonic units. In this respect, our data argue that information about irradiance is not segregated to a particular subset of dLGN units (as described for other visual features; e.g., direction, motion), but appears diffusely across the population.

The relationship between irradiance and firing rate that we observe is overwhelmingly positive. Thus, we found only a small fraction of units whose firing was lower at the end of the ramp, and even fewer with a negative linear change in firing. Others have reported more numerous negative luxotonic activity using less natural stimuli (9, 12) but our data are consistent with data showing irradiance-dependent increases in glucose metabolism of the dLGN (37, 38). The positive luxotonic behavior we observe is found not only in units with ON responses to abrupt increments in light, but also those with OFF responses. In this way, our data indicate that dLGN units with phasic OFF responses can receive a sustained ON signal. This finding fits with a growing appreciation that the distinction between ON and OFF channels is less clear than previously imagined (34, 39–41).

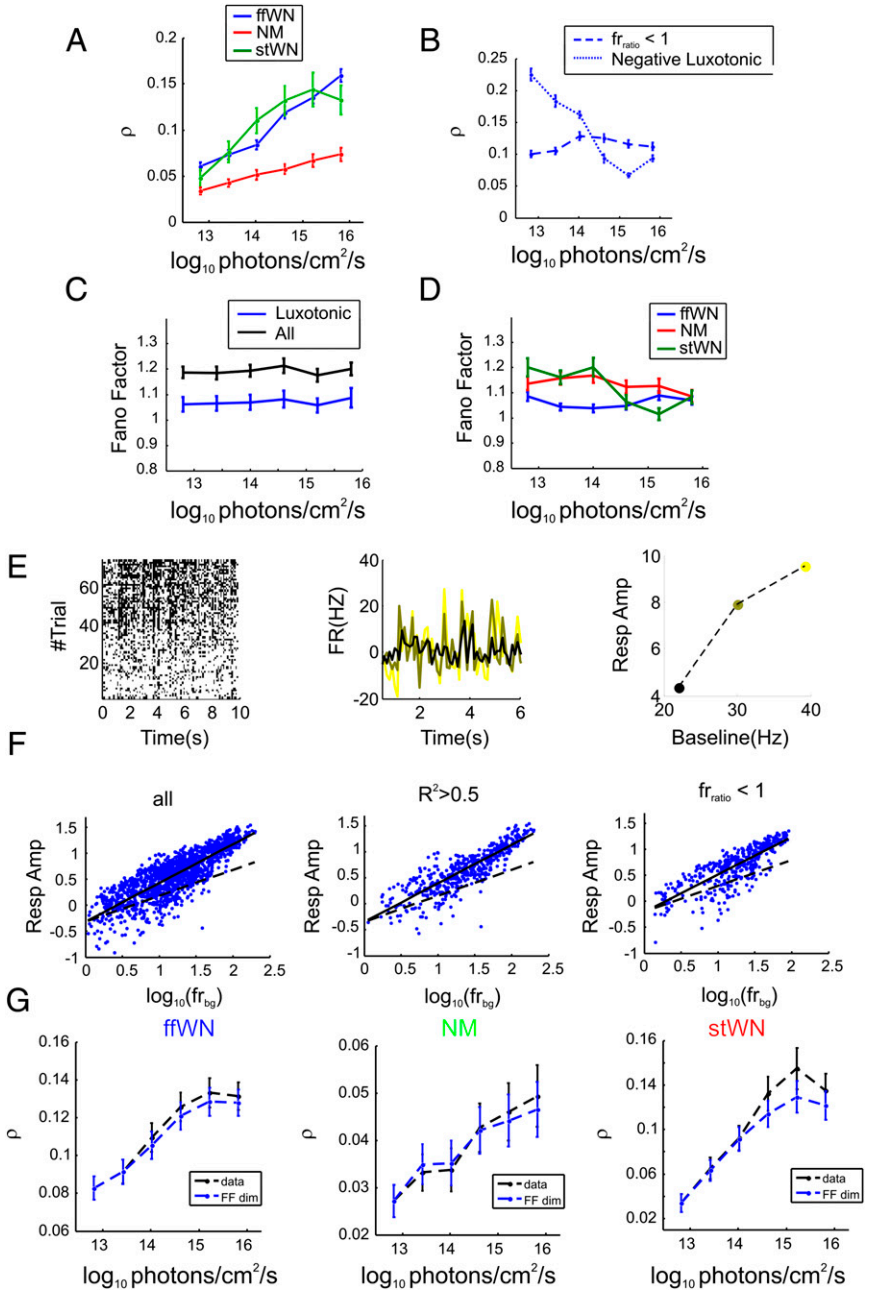

Fig. 5. Luxotonic responses improve reproducibility of fast-evoked responses. (*A*) Trial-to-trial correlation (time bin duration = 200 ms) increases as function of irradiance for all stimuli (ffWN, NM, stWN). (*B*) Trial-to-trial correlation is unaltered in units lacking an irradiance-dependent increment in firing rate ($P = 0.31$, $n = 73$) and is reduced at high irradiance levels for units with a negative luxotonic response. (*C*) Population-averaged Fano factor is constant across irradiance levels both for strongly luxotonic units and for the whole population of dLGN units. (*D*) Fano factor across irradiance levels for ffWN, NM, and stWN. (*E*) Binarized trial bin counts (*Left*) average fast-evoked responses (*Center*), and relation between baseline firing and power of evoked responses (*Right*) for a representative unit. (*F*) The response amplitude has a power law relation with baseline firing for all dLGN units (*Left*), luxotonic units (*Center*), and units lacking a firing rate increase across the ramp (*Right*). Solid lines represent the fit, dashed lines represent power law exponent = 0.5. (*G*) Fano factor manipulation: for each unit the Fano factor values at all irradiance levels are replaced by the ones calculated at the dimmest condition. Then ρ is estimated by using *SI Appendix*, Eq. **4**. The difference between original and Fano factor-manipulated ρ estimates (respectively, black and blue error bars) represents the contribution of firing rate regularization.

Functions of Luxotonic Activity. What functions could the diffuse increase in firing perform? One obvious possibility is that it encodes the changing background light intensity for higher visual processes, including perception. Psychophysical studies confirm that irradiance can be accurately perceived under a wide range of circumstances (42–46). Indeed, although humans perceive stimuli with very slowly changing irradiance (as presented here) as invariant, they do eventually report that the scene has gotten brighter. However, given the energetic expense of spiking, it is hard to imagine that such a widespread change in activity across the dLGN represents the most efficient method of representing this aspect of the visual scene. This raises the question of whether luxotonic behavior serves an additional function.

Human visual performance increases over a wide range of irradiances (47–49). This improvement likely originates in part with reductions in photon noise and with light adaptation in visual

circuits (5, 31, 50–52). However, our study reveals that luxotonic activity may also make an important contribution. We find that across all dLGN units, the amplitude of fast visual responses is positively correlated with maintained firing rate. The exponent of this relationship is sufficient to provide substantial improvements in response reproducibility as a function of baseline firing rate. Thus, cells showing increases in firing rate across the ramp also show improvements in fast-response reproducibility, whereas the opposite occurs in those cells whose firing rate falls.

Taking into account the likely energetic expense of luxotonic activity, we suggest that its major function may therefore be active resource allocation. By increasing the excitability of the early visual system as dawn progresses, luxotonic activity increases the number of spikes available to transmit high-frequency visual information and thus enhances response reproducibility (Fig. 5 *F* and *G*).

Origins of Luxotonic Responses. We present several lines of evidence that, under the conditions studied here, luxotonic behavior originates in part from melanopsin photoreception. We first show that melanopsin knockout mice show very little increase in firing across the ramp. This might be expected as the range of irradiances tested here are largely within the sensitivity range of melanopsin. However, in view of the evidence that retinal development is disrupted in melanopsin knockout mice (26–28), we wished to confirm this result with a more acute inhibition of ipRGC activity. To that end, we turned to chemogenetic technology. Using viral gene targeting, we were able to express the inhibitory DREADD receptor hM4D(Gi) in around 30% of ipRGCs. This level of expression is sufficient to allow CNO to partially inhibit a known output of ipRGCs (the pupil light reflex). Accordingly, we find that CNO partially inhibited luxotonic activity in the dGLN, reducing the linearity and reproducibility of irradiance-driven increases in firing across the dLGN.

The disruption in luxotonic activity following melanopsin knockout and chemogenetic inhibition of ipRGCs is consistent with the hypothesis that melanopsin influences luxotonic activity. However, neither dataset provides a very clear indication of its exact contribution. Addressing that question requires a more precise manipulation of melanopsin activity. We have achieved this by using the principles of receptor silent substitution to produce a second version of the irradiance ramp that is cone-isoluminant but whose effective irradiance for melanopsin is reduced by 10×. If luxotonic activity were solely driven by cones then the response to this MelLow ramp would be equivalent to that of our standard Daylight ramp. If it were solely produced by melanopsin, then the increase in firing should simply be delayed by 4 min (the time taken to increase irradiance by 1 log unit). In fact, we observe a net discontinuity in the luxotonic response to the MelLow ramp (Fig. 2*N*), indicating that both cones and melanopsin are relevant under these conditions. Whereas in the Daylight condition luxotonic activity takes the form of a seamless increase in firing across the ramp, in MelLow there are two phases to the response. At lower irradiances, firing increases gradually and appears to approach an intermediate asymptote before subsequently increasing more rapidly (Fig. 2*N*).

These data are consistent with current models of irradiance coding by the mammalian retina in which melanopsin becomes increasingly influential as brightness increases. At lower irradiances and, by extension, at early points in the twilight progression, any luxotonic activity would likely rely upon cones and rods.

Summary

Melanopsin photoreception was discovered in attempts to understand circadian photoentrainment and has since been shown to contribute to a wide variety of accessory visual responses. The current dataset contributes to a growing appreciation of its contribution to more conventional perceptual vision as well. Previous studies have shown that melanopsin contributes to setting pupil size (53), and discriminating global brightness (54). Melanopsin is expressed in a subset of retinal ganglion cells whose anatomy and physiology is consistent with a role in spatial discrimination, and melanopsin knockout mice have impaired contrast sensitivity (55). Finally, studies in both humans and mice indicate that melanopsin supports network light adaptation in the early visual system (31, 56, 57). The data presented here reveal an additional way in which melanopsin could influence performance across any aspect of vision. Thus, simply by supporting irradiance-dependent increases in excitability across the dLGN, it increases the reliability of fast visual responses.

Methods

Electrophysiology. Experiments were in accordance with the Animals, Scientific Procedures Act of 1986 (United Kingdom), and approved by the UoM ethical review committee. Animals were kept in a 12-h dark/light cycle at a temperature of 22 °C with food and water available ad libitum. Recordings were undertaken in their subjective day. Except where otherwise stated, experiments were performed on adult (3–6 mo) mice carrying a knock-in of the human red cone opsin (*Opn1mw*^{R}) (58). Intravitreal injections of AAV2-hSyn-DIO-hM4D(Gi)-mCherry vector (2.3^{13} genomic particles per milliliter; The UNC Vector Core) were done in *Opn4*$^{Cre/+}$ mice, as previously reported (59) and used hyaluronan lyase and heparinase III (200 U each) to maximize retinal penetration. Mice were allowed at least 6 wk to recover before being used in in vivo studies. Administration of CNO (Abcam, ab141704) was always performed via an intraperitoneal route (10 mg/kg).

In Vivo. Animals were anesthetized with an intraperitoneal injection of urethane [1.6 g/kg; 30% (wt/vol); Sigma-Aldrich]. Atropine and mineral oil (Sigma-Aldrich) were applied to the recording eye. The mice were placed into a stereotaxic frame to keep a fixed-head position and into a bite bar to provide further head support and electrical grounding. Core body temperature was maintained at 37 °C throughout recording with a homeothermic heat mat (Harvard Apparatus). Extracellular signals were acquired using a Recorder64 system (Plexon), and were amplified (3,500×), high-pass–filtered (300 Hz), and digitized at 40 kHz. Spikes were sorted offline by using Offline Sorter (Plexon).

Immunochistochemistry. Immunohistochemistry was performed as previously described in Hughes et al. (60) on retinal whole mounts and sections fixed in methanol-free 4% (wt/vol) paraformaldehyde. The primary antibodies used in these studies include rabbit anti-dsRed (Clontech 632496; 1:1,000) and chicken anti-GFP (Abcam ab13970; 1:1,000). The secondary antibodies were Alexa 488 conjugated donkey anti-chicken (Jackson Immunoresearch) and Alexa 546 conjugated donkey anti-rabbit (Life Technologies) at 1:200. Images were collected on a Leica TCS SP5 AOBS inverted confocal using a 40×/0.50 Plan Fluotar objective and 1.5× confocal zoom.

Pupillometry. Consensual pupil constriction to a 10-s full field white (150 W Metal-halide lamp; Phillips) pulse was measured as described previously (61).

Visual Stimuli. Full-field and spatially structured stimuli were presented using two different systems depicted in *SI Appendix*, Figs. S14 and S15. In all cases, spectral composition was defined by independent control of colored LEDs and calibrated using a spectroradiometer (Bentham Instruments), which measured the power in milliwatt per square centimeter at wavelengths between 300 and 800 nm. The effective photon flux for any photopigment was calculated as previously described (31) by weighting spectral irradiance according to the spectral sensitivity of cones, rods, and melanopsin. The template functions for individual mouse opsins were calculated as function of λ_{max} by using the Govardovskii equations (62) and corrected for lens transmission (63).

The irradiance ramp was designed is order to capture the salient aspects of a dawn transition in Manchester, while acknowledging that on the one hand, it lacked the very slowest changes found in the natural day, and on the other, that dawn progresses faster nearer the equator (Fig. 2*A*). Its spectral composition recreated the balance of mouse cone, rod, and melanopsin excitations typical of natural light (Daylight spectrum) (31). The irradiance values at its brightest condition were 0.14×10^{15} photons per square centimeter per second (s-cones), 2.24×10^{15} photons per square centimeter per second (melanopsin), 2.03×10^{15} photons per square centimeter per second (rods), and 2.25×10^{15} photons per square centimeter per second (l-cones). The ramp recreated corneal irradiances across the dawn transition, but did not

reach the brightest daylight levels to allow for ~20× reduction in retinal irradiance because of pupil constriction (53) that was blocked in our in vivo preparations. The MelLow spectrum provided the same excitation for s-cones and l-cones but a fivefold decrease in rod excitation (–0.67 Michelson contrast) and a 10-fold decrease in melanopsin excitation (–0.82 Michelson contrast). For the NM and the stWN stimuli, irradiance at its brightest was 0.6×10^{14} photons per square centimeter per second (s-cones), 4.9×10^{14} photons per square centimeter per second (melanopsin), 4.7×10^{14} photons per square centimeter per second (rods), and 3.6×10^{14} photons per square centimeter per second (l-cones).

Further details about the design and implementation of full field and spatially structured stimuli can be found in the text of the *SI Appendix* and in *SI Appendix*, Figs. S13–S15.

Analyses.

Linear fit analysis. Irradiance sensitivity was measured by using the R^2 values obtained by fitting the firing rate responses as a log-linear function of the irradiance. The bin duration we used to estimate firing rate was set at 30 s. The bin choice however was not critical. R^2 was estimated as $1 - \Sigma_{\#bin}(FR - FR_{fit})^2 / \Sigma_{\#bin}(FR - \langle FR \rangle)^2$. The R^2 metric takes into account both neuronal random variability and the gain/slope of the irradiance–firing rate relation. Neurons with large R^2 values will feature a low firing-rate variability [relatively small values of $\Sigma_{\#bin}(FR - FR_{fit})^2$] and a large irradiance-related gain [relatively large values of $\Sigma_{\#bin}(FR - \langle FR \rangle)^2$].

Firing-rate comparison and normalization. To estimate the relative increase in firing rate, we computed the ratio between the lowest and highest irradiance levels (data were pooled at half-log unit steps in irradiance). We defined this measure as fr_{ratio}. To analyze and compare population responses the firing rate of each unit was as $FR_{norm} = [FR - \min(FR)]/[\max(FR) - \min(FR)]$. This normalization was applied throughout the whole of *Results*. For Daylight – MelLow response comparisons, we used only those units that were consistently classified as strongly luxotonic ($R^2 > 0.5$), both for the first and the second presentation of the Daylight ramp ($n = 89$).

Reverse correlation analysis. The ffWN stimulus was divided into six blocks, each block encompassing 0.5 log-unit range of irradiance. For each unit the spike-triggered average (STA) was then estimated separately for each block (time bin = 10 ms, window of time before spikes = 0.5 s) by using standard techniques (64).

STA clustering. All STAs across blocks (see above) and across units were pooled together and the principal components were estimated. By using the scores associated with the first three components, each unit was therefore defined by 18 values (3 scores × 6 trial blocks). Clustering was then performed by using the *k*-means algorithm. For this process we used the correlation distance to capture similarities in the irradiance dependent modification of the STA shapes across the trial blocks. The clustering was repeated 100 times to avoid suboptimal results because of the presence of local minima. The whole procedure was repeated by setting different cluster numbers (2–7). The optimal number of clusters was then defined by the lowest average silhouette value.

Reproducibility analysis. The trial-to-trial correlation was estimated by using Pearson's linear correlation. The discretized spike trains collected from all trials were divided into six blocks corresponding to the different irradiance levels (0.5 log-unit steps) and the average Pearson's linear correlation for each block was estimated. To reduce the variance of the estimate for each block we used a jack-knife procedure. Only those cells that emitted spikes in at least 95% of the trials in each blocks were used (98%, $n = 215$; 83%, $n = 93$; 100%, $n = 46$; light responsive units for ffWN, NM, and stWN in dLGN).

The estimation of response amplitude and baseline firing are explained and validated in the text of *SI Appendix* and in *SI Appendix*, Figs. S11 and S12.

Fano factor analysis. The Fano factor index was estimated following Churchland et al. (65). During the simple ramp stimulus the response was divided into nonoveralapping blocks (125 s, time bin = 0.1 s). For each block the mean and variance in firing rates were calculated in 10 subblocks (12.5 s) and a scatterplot was generated by using variance as the dependent variable. Then the Fano factor was estimated as the slope of the weighted least-square linear fit and the line was constrained to pass through zero (Matlab function lscov.m). During ffWN, NM, and stWN, the Fano factor was estimated for each trial block as for the Pearson's correlation.

Notation for significance of statistical tests. Throughout all graphs we always used the following notation for the statistical tests: $*P < 0.01$; $**P < 0.005$; $***P < 0.001$; $****P < 0.0005$; $*****P$ = all lower values.

All of the analyses were performed by using Matlab software (MATLAB 2011a, MathWorks).

ACKNOWLEDGMENTS. We thank Peter March and Roger Meadows of the Faculty of Life Sciences Bioimaging facility for their help with the microscopy; and for the generous donation of mouse lines, Samer Hattar (*Opn4*^{cre}, *Opn4*$^{-/-}$), King-Wai Yau (*Opn4*$^{-/-}$), and Jeremy Nathans (*Opn1mw*^{R}), all of Johns Hopkins University. This work was supported by grants from European Research Council Grant MeloVision (to R.J.L.); and Biotechnology and Biological Sciences Research Council Grants BB/I007296/1 (to R.J.L.) and BB/I017836/1 (to T.M.B.). The Bioimaging Facility microscopes used in this study were purchased with grants from the Biotechnology and Biological Sciences Research Council, Wellcome Trust, and the University of Manchester Strategic Fund.

1. Bloomfield SA, Völgyi B (2009) The diverse functional roles and regulation of neuronal gap junctions in the retina. *Nat Rev Neurosci* 10(7):495–506.
2. Burkhardt DA (1994) Light adaptation and photopigment bleaching in cone photoreceptors in situ in the retina of the turtle. *J Neurosci* 14(3 Pt 1):1091–1105.
3. Dowling JE (1960) Chemistry of visual adaptation in the rat. *Nature* 188:114–118.
4. Dunn FA, Lankheet MJ, Rieke F (2007) Light adaptation in cone vision involves switching between receptor and post-receptor sites. *Nature* 449(7162):603–606.
5. Enroth-Cugell C, Lennie P (1975) The control of retinal ganglion cell discharge by receptive field surrounds. *J Physiol* 247(3):551–578.
6. Perlman I, Normann RA (1998) Light adaptation and sensitivity controlling mechanisms in vertebrate photoreceptors. *Prog Retin Eye Res* 17(4):523–563.
7. Pugh EN, Jr, Nikonov S, Lamb TD (1999) Molecular mechanisms of vertebrate photoreceptor light adaptation. *Curr Opin Neurobiol* 9(4):410–418.
8. Witkovsky P (2004) Dopamine and retinal function. *Doc Ophthalmol* 108(1):17–40.
9. Barlow HB, Levick WR (1969) Changes in the maintained discharge with adaptation level in the cat retina. *J Physiol* 202(3):699–718.
10. Gur M (1987) Intensity coding and luxotonic activity in the ground squirrel lateral geniculate nucleus. *Vision Res* 27(12):2073–2079.
11. Jacobs GH, Yolton RL (1970) Center-surround balance in receptive fields of cells in the lateral geniculate nucleus. *Vision Res* 10(11):1127–1144.
12. Kayama Y, Riso RR, Bartlett JR, Doty RW (1979) Luxotonic responses of units in macaque striate cortex. *J Neurophysiol* 42(6):1495–1517.
13. Marrocco RT (1972) Maintained activity of monkey optic tract fibers and lateral geniculate nucleus cells. *Vision Res* 12(6):1175–1181.
14. Sakmann B, Creutzfeldt OD (1969) Scotopic and mesopic light adaptation in the cat's retina. *Pflugers Arch* 313(2):168–185.
15. Frishman LJ, Levine MW (1983) Statistics of the maintained discharge of cat retinal ganglion cells. *J Physiol* 339:475–494.
16. Levine MW, Troy JB (1986) The variability of the maintained discharge of cat dorsal lateral geniculate cells. *J Physiol* 375:339–359.
17. Lowen SB, Ozaki T, Kaplan E, Saleh BE, Teich MC (2001) Fractal features of dark, maintained, and driven neural discharges in the cat visual system. *Methods* 24(4):377–394.
18. Baden T, Berens P, Bethge M, Euler T (2013) Spikes in mammalian bipolar cells support temporal layering of the inner retina. *Curr Biol* 23(1):48–52.
19. Li W, DeVries SH (2006) Bipolar cell pathways for color and luminance vision in a dichromatic mammalian retina. *Nat Neurosci* 9(5):669–675.
20. Odermatt B, Nikolaev A, Lagnado L (2012) Encoding of luminance and contrast by linear and nonlinear synapses in the retina. *Neuron* 73(4):758–773.
21. Oesch NW, Diamond JS (2011) Ribbon synapses compute temporal contrast and encode luminance in retinal rod bipolar cells. *Nat Neurosci* 14(12):1555–1561.
22. Normann RA, Perlman I (1979) The effects of background illumination on the photoresponses of red and green cones. *J Physiol* 286:491–507.
23. Valeton JM, van Norren D (1983) Light adaptation of primate cones: An analysis based on extracellular data. *Vision Res* 23(12):1539–1547.
24. Dacey DM, et al. (2005) Melanopsin-expressing ganglion cells in primate retina signal colour and irradiance and project to the LGN. *Nature* 433(7027):749–754.
25. Storchi R, et al. (2010) Modeling neuronal ensemble firing activity through intermittent chaos. *2010 IEEE Fifth International Conference on Bio-Inspired Computing: Theories and Applications* (IEEE, Piscataway, NJ), pp. 1593–1598.
26. Johnson J, et al. (2010) Melanopsin-dependent light avoidance in neonatal mice. *Proc Natl Acad Sci USA* 107(40):17374–17378.
27. Rao S, et al. (2013) A direct and melanopsin-dependent fetal light response regulates mouse eye development. *Nature* 494(7436):243–246.
28. Renna JM, Weng S, Berson DM (2011) Light acts through melanopsin to alter retinal waves and segregation of retinogeniculate afferents. *Nat Neurosci* 14(7):827–829.
29. Armbruster BN, Li X, Pausch MH, Herlitze S, Roth BL (2007) Evolving the lock to fit the key to create a family of G protein-coupled receptors potently activated by an inert ligand. *Proc Natl Acad Sci USA* 104(12):5163–5168.
30. Krashes MJ, et al. (2011) Rapid, reversible activation of AgRP neurons drives feeding behavior in mice. *J Clin Invest* 121(4):1424–1428.
31. Allen AE, et al. (2014) Melanopsin-driven light adaptation in mouse vision. *Curr Biol* 24(21):2481–2490.
32. Brown TM, et al. (2010) Melanopsin contributions to irradiance coding in the thalamo-cortical visual system. *PLoS Biol* 8(12):e1000558.
33. Invergo BM, Dell'Orco D, Montanucci L, Koch KW, Bertranpetit J (2014) A comprehensive model of the phototransduction cascade in mouse rod cells. *Mol Biosyst* 10(6):1481–1489.
34. Tikidji-Hamburyan A, et al. (2015) Retinal output changes qualitatively with every change in ambient illuminance. *Nat Neurosci* 18(1):66–74.

35. Grubb MS, Thompson ID (2003) Quantitative characterization of visual response properties in the mouse dorsal lateral geniculate nucleus. *J Neurophysiol* 90(6): 3594–3607.
36. Howarth M, Walmsley L, Brown TM (2014) Binocular integration in the mouse lateral geniculate nuclei. *Curr Biol* 24(11):1241–1247.
37. Cooper RM (2002) Diffuse light increases metabolic activity in the lateral geniculate nucleus, visual cortex, and superior colliculus of the cone-dominated ground squirrel visual system. *Vision Res* 42(27):2899–2907.
38. Cooper RM, Thurlow GA (1991) [2-14C]deoxyglucose uptake in rat visual system during flashing-diffuse and flashing-pattern stimulation over a 6 log range of luminance. *Exp Neurol* 113(1):79–84.
39. Farrow K, et al. (2013) Ambient illumination toggles a neuronal circuit switch in the retina and visual perception at cone threshold. *Neuron* 78(2):325–338.
40. Geffen MN, de Vries SE, Meister M (2007) Retinal ganglion cells can rapidly change polarity from Off to On. *PLoS Biol* 5(3):e65.
41. Moore BD, 4th, Kiley CW, Sun C, Usrey WM (2011) Rapid plasticity of visual responses in the adult lateral geniculate nucleus. *Neuron* 71(5):812–819.
42. Barlow RB, Jr, Verrillo RT (1976) Brightness sensation in a ganzfeld. *Vision Res* 16(11): 1291–1297.
43. Bolanowski SJ, Jr, Doty RW (1987) Perceptual "blankout" of monocular homogeneous fields (Ganzfelder) is prevented with binocular viewing. *Vision Res* 27(6):967–982.
44. Knau H (2000) Thresholds for detecting slowly changing Ganzfeld luminances. *J Opt Soc Am A Opt Image Sci Vis* 17(8):1382–1387.
45. Knau H, Spillmann L (1997) Brightness fading during Ganzfeld adaptation. *J Opt Soc Am A Opt Image Sci Vis* 14(6):1213–1222.
46. Schouten G, Blommaert FJ (1995) Brightness constancy in a Ganzfeld environment. *Percept Psychophys* 57(7):1012–1022.
47. Sheedy JE, Bailey IL, Raasch TW (1984) Visual acuity and chart luminance. *Am J Optom Physiol Opt* 61(9):595–600.
48. Sloan LL (1968) The photopic acuity-luminance function with special reference to parafoveal vision. *Vision Res* 8(7):901–911.
49. Wilcox WW (1932) The basis of the dependence of visual acuity on illumination. *Proc Natl Acad Sci USA* 18(1):47–56.
50. Bisti S, Clement R, Maffei L, Mecacci L (1977) Spatial frequency and orientation tuning curves of visual neurones in the cat: Effects of mean luminance. *Exp Brain Res* 27(3-4): 335–345.
51. Mante V, Frazor RA, Bonin V, Geisler WS, Carandini M (2005) Independence of luminance and contrast in natural scenes and in the early visual system. *Nat Neurosci* 8(12):1690–1697.
52. Sagdullaev BT, McCall MA (2005) Stimulus size and intensity alter fundamental receptive-field properties of mouse retinal ganglion cells in vivo. *Vis Neurosci* 22(5): 649–659.
53. Lucas RJ, Douglas RH, Foster RG (2001) Characterization of an ocular photopigment capable of driving pupillary constriction in mice. *Nat Neurosci* 4(6):621–626.
54. Brown TM, et al. (2012) Melanopsin-based brightness discrimination in mice and humans. *Curr Biol* 22(12):1134–1141.
55. Schmidt TM, et al. (2014) A role for melanopsin in alpha retinal ganglion cells and contrast detection. *Neuron* 82(4):781–788.
56. Hankins MW, Lucas RJ (2002) The primary visual pathway in humans is regulated according to long-term light exposure through the action of a nonclassical photopigment. *Curr Biol* 12(3):191–198.
57. Zhang DQ, et al. (2008) Intraretinal signaling by ganglion cell photoreceptors to dopaminergic amacrine neurons. *Proc Natl Acad Sci USA* 105(37):14181–14186.
58. Smallwood PM, et al. (2003) Genetically engineered mice with an additional class of cone photoreceptors: Implications for the evolution of color vision. *Proc Natl Acad Sci USA* 100(20):11706–11711.
59. Cehajic-Kapetanovic J, Le Goff MM, Allen A, Lucas RJ, Bishop PN (2011) Glycosidic enzymes enhance retinal transduction following intravitreal delivery of AAV2. *Mol Vis* 17:1771–1783.
60. Hughes S, et al. (2013) Nonuniform distribution and spectral tuning of photosensitive retinal ganglion cells of the mouse retina. *Curr Biol* 23(17):1696–1701.
61. Enezi Ja, et al. (2011) A "melanopic" spectral efficiency function predicts the sensitivity of melanopsin photoreceptors to polychromatic lights. *J Biol Rhythms* 26(4): 314–323.
62. Govardovskii VI, Fyhrquist N, Reuter T, Kuzmin DG, Donner K (2000) In search of the visual pigment template. *Vis Neurosci* 17(4):509–528.
63. Jacobs GH, Williams GA (2007) Contributions of the mouse UV photopigment to the ERG and to vision. *Doc Ophthalmol* 115(3):137–144.
64. Chichilnisky EJ (2001) A simple white noise analysis of neuronal light responses. *Network* 12(2):199–213.
65. Churchland MM, et al. (2010) Stimulus onset quenches neural variability: A widespread cortical phenomenon. *Nat Neurosci* 13(3):369–378.
66. Lucas RJ, et al. (2014) Measuring and using light in the melanopsin age. *Trends Neurosci* 37(1):1–9.